Regimes of Terminal Motion of Sliding Spinning Disks

P. D. Weidman[1] and C. P. Malhotra[2]

[1]*Department of Mechanical Engineering, University of Colorado, Boulder, Colorado 80390-0427, USA*
[2]*Tata Research Development and Design Centre, 54/B HIE, Pune 411013, India*

(Received 12 May 2005; revised manuscript received 15 September 2005; published 23 December 2005)

Analysis of the frictional motion of a uniform circular disk of radius R sliding and spinning on a horizontal table reported by Farkas *et al.* [Phys. Rev. Lett. **90**, 248302 2003] shows that the disk always stops sliding and spinning at the same instant with a terminal speed ratio $\epsilon_0 = v/R\omega = 0.653$. We show that different terminal behaviors can be found when one considers the motion of a two-tier disk with lower section thickness H_1 and radius R_1, and upper section thickness H_2 and radius R_2. The terminal motion may be analyzed in terms of the normalized radius of gyration k. It is found that while translation and rotation cease simultaneously, their terminal ratio ϵ_0 either vanishes when $k > \sqrt{2/3}$, is a nonzero constant when $1/2 < k < \sqrt{2/3}$, or diverges when $k < 1/2$. Experiments performed with plastic disks sliding on a nylon fabric stretched over a horizontal plate qualitatively corroborate the three different types of terminal motion.

DOI: 10.1103/PhysRevLett.95.264303 PACS numbers: 45.40.−f, 46.55.+d, 81.40.Pq

Farkas *et al.* [1], motivated by problems in the compaction of a dry powder of faceted particles [2–4], describe a new and interesting aspect of the motion of a circular disk sliding and spinning across a flat surface with Coulomb friction. For a disk of radius R sliding with velocity v and spinning with angular rotation rate ω, it was proven that sliding and spinning cease at the same instant. Moreover, the coupling between the sliding and spinning motions continuously focuses the *speed ratio* $\epsilon = v/\omega R$ toward its terminal value $\epsilon_0 = 0.653$, regardless of the nonzero initial conditions on v and ω. The analysis is predicated on a near uniform normal stress acting across the surface of the disk during deceleration. The above results have been reviewed by Halsey [5].

Our interest in this problem stemmed from demonstrations of the phenomenon at coffee shops and beer parlors. Coins and bottle tops indeed appear to stop sliding and spinning at the same time. But when an eyeglass case was launched across a table, it inevitably stopped translating first, and then spun down to rest. This was not attributed to the oblong shape of the case, but rather to the fact that it was slightly bowed concave upward, and hence its contact with the table is localized to a small area at the center of the case. This provided the motivation to study alternative geometries that will (i) stop sliding first and then spin down to rest, or (ii) stop spinning first and then slide to rest. The vehicle of demonstration is a small aspect ratio two-tier disk, although, as will be noted later, the results obtained are quite general.

The notation in [1] is closely followed to compute the force and torque acting on *generic* sliding and spinning disks retarded by dry friction. The Coulomb friction law states that the magnitude of the local friction force is proportional to the local normal force and acts opposite to the local relative velocity between surfaces in contact. For a uniform normal stress, the friction force on a sliding-spinning disk is given by

$$\boldsymbol{F} = -\frac{\mu F_n}{A}\int_A \frac{\boldsymbol{v}+\boldsymbol{\omega}\times\boldsymbol{r}}{|\boldsymbol{v}+\boldsymbol{\omega}\times\boldsymbol{r}|}\,dS, \tag{1}$$

where $\boldsymbol{r}$ is the radius vector from the center of the disk, $\boldsymbol{v}$ is the linear velocity of the disk, $\boldsymbol{\omega}$ its angular rotation rate, μ the friction coefficient, A the disk area in contact with the horizontal surface, and $F_n = mg$ is the normal force where m is the mass of the disk and g is the gravitational acceleration. Similarly, the friction torque is

$$\boldsymbol{T} = -\frac{\mu F_n}{A}\int_A \boldsymbol{r}\times\frac{\boldsymbol{v}+\boldsymbol{\omega}\times\boldsymbol{r}}{|\boldsymbol{v}+\boldsymbol{\omega}\times\boldsymbol{r}|}\,dS. \tag{2}$$

Evaluation of (1) and (2) for a uniform disk of radius R by Farkas *et al.* [1] gives $\boldsymbol{F} = -F_n\mathcal{F}(\epsilon)\mathbf{e}_v$ and $\boldsymbol{T} = -F_nR\mathcal{T}(\epsilon)\mathbf{e}_\omega$, where $\mathbf{e}_v = \boldsymbol{v}/v$ is the unit vector in the direction of translation, $\mathbf{e}_\omega = \boldsymbol{\omega}/\omega$ is the unit vector normal to the disk, and $\mathcal{F}(\epsilon)$ and $\mathcal{T}(\epsilon)$ are given in terms of complete elliptic integrals $K(\epsilon)$ and $E(\epsilon)$. The functions $\mathcal{F}(\epsilon)$ and $\mathcal{T}(\epsilon)$ reported in [1] are in error, even though the plots given in their Fig. 2 are correct. The correct results using the notation in [6] are

$$\mathcal{F}(\epsilon) = \begin{cases} \frac{4}{3\epsilon}\frac{(\epsilon^2+1)E(\epsilon^2)+(\epsilon^2-1)K(\epsilon^2)}{\pi} & \epsilon \le 1 \\ \frac{4}{3\epsilon}\frac{(\epsilon^2+1)E(1/\epsilon^2)+(\epsilon^2-1)K(1/\epsilon^2)}{\pi} & \epsilon \ge 1 \end{cases} \tag{3a}$$

and

$$\mathcal{T}(\epsilon) = \begin{cases} \frac{4}{9}\frac{(4-2\epsilon^2)E(\epsilon^2)+(\epsilon^2-1)K(\epsilon^2)}{\pi} & \epsilon \le 1 \\ \frac{4\epsilon}{9}\frac{(4-2\epsilon^2)E(1/\epsilon^2)+(2\epsilon^2-5+3/\epsilon^2)K(1/\epsilon^2)}{\pi} & \epsilon \ge 1 \end{cases}. \tag{3b}$$

The motion of the disks is governed by the scalar linear and angular momentum equations

$$F = m\frac{dv}{dt}, \tag{4a}$$

$$T = I\frac{d\omega}{dt}, \tag{4b}$$

in which I is the polar moment of inertia of the disk.

In the axisymmetric two-tier disk of uniform density ρ being considered, the lower and upper tiers have radii R_1 and R_2 and thicknesses H_1 and H_2, respectively. Hence this geometry is characterized by two dimensionless parameters, the radius ratio $\eta = R_1/R_2$ and the thickness ratio $\lambda = H_1/H_2$. For this configuration

$$m = \pi\rho(H_1R_1^2 + H_2R_2^2), \qquad I = \frac{\pi\rho}{2}(H_1R_1^4 + H_2R_2^4). \tag{5}$$

Evaluation of integrals (1) and (2) gives

$$\boldsymbol{F} = -\mu mg\mathcal{F}(\epsilon)\mathbf{e}_v, \tag{6a}$$

$$\boldsymbol{T} = -\mu mgR_1\mathcal{T}(\epsilon)\mathbf{e}_\omega, \tag{6b}$$

where $\epsilon = v/\omega R_1$ is the speed ratio. Using the results in (6), the governing equations of motion (4) are

$$\frac{dv}{dt} = -\mu g\mathcal{F}(\epsilon), \tag{7a}$$

$$\frac{d\omega}{dt} = -\frac{2\mu g}{R_2}\left(\frac{\eta^2\lambda + 1}{\eta^4\lambda + 1}\right)\eta\mathcal{T}(\epsilon) \tag{7b}$$

Scaling $(v,\ \omega,\ t)$ with $(\mu\sqrt{R_1 g},\ \mu\sqrt{g/R_1},\ \sqrt{R_1/g})$ we obtain

$$\frac{dv^*}{dt^*} = -\mathcal{F}(\epsilon), \tag{8a}$$

$$\frac{d\omega^*}{dt^*} = -\frac{2\eta^2(\eta^2\lambda + 1)}{(\eta^4\lambda + 1)}\mathcal{T}(\epsilon), \tag{8b}$$

where variables with an asterisk are dimensionless. Dividing (8a) by (8b) and making the change of variables $x = -\ln\omega^*$ gives

$$f(\epsilon, k) \equiv \frac{d\epsilon}{dx} = \epsilon - k^2\frac{\mathcal{F}(\epsilon)}{\mathcal{T}(\epsilon)}. \tag{9}$$

Using (5) we find that k in (9) is, in fact, the radius of gyration of the composite disk normalized by the radius of the contact disk, viz.

$$k = \frac{1}{R_1}\sqrt{\frac{I}{m}} = \sqrt{\frac{(\eta^4\lambda + 1)}{2\eta^2(\eta^2\lambda + 1)}}. \tag{10}$$

Consequently, the η-λ two-parameter family of solutions may be analyzed solely in terms of the single parameter k. Using MATHEMATICA [7] we plot in Fig. 1 curves $f(\epsilon)$ at selected values of k, and note that the range of k is $[0, \infty]$. The curve for $k = k_0 = 1/\sqrt{2}$ corresponds to the pure disk with attractive fixed point at the $\epsilon_0 = 0.653$ zero crossing of $f(\epsilon)$. We investigate the terminal motion of two-tier disks by increasing or decreasing k from this value. As k increases, the fixed point at $\epsilon_0 = 0.653$ slides to the left and eventually hits the origin when $f(\epsilon)$ becomes tangent to the horizontal axis as indicated by the dashed curve for $k_1 = \sqrt{2/3}$. Increasing k above this critical value gives curves pinned to the origin such as those marked k_2 and k_3 in Fig. 1. Thus for all values $k > \sqrt{2/3}$, the fixed point lies at $\epsilon_0 = 0$.

We now decrease k below the pure disk value $k = k_0$. Then the attractive fixed point slides to the right to the zero crossing of the curve marked k_{-1}. With further decrease in k, the fixed point moves off to infinity when $k = k_{-2} = 1/2$ displayed as the dash-dot-dash curve in Fig. 1, at which point $f(\epsilon)$ is tangent to the horizontal axis at infinity. At still lower values, like k_{-3} and k_{-4}, the $f(\epsilon)$ curves lift off the horizontal axis with ever increasing slope at the origin. Thus for all $k < 1/2$, the fixed point lies at $\epsilon_0 = \infty$.

Setting $f(\epsilon_0, k) = 0$ in (9) furnishes the connection between the radius of gyration and the terminal values ϵ_0, namely $k = \sqrt{\epsilon_0\mathcal{T}(\epsilon_0)/\mathcal{F}(\epsilon_0)}$. This variation of k with ϵ_0 is shown in Fig. 2 in which the dot represents the pure disk result.

Consider the fundamental state to be one for which ϵ_0 is a nonzero constant. Transitions from this state to the two other terminal motion states are readily found in η-λ space. For example, the transition to terminal motion regime $\epsilon_0 = 0$ is obtained by setting $k = \sqrt{2/3}$ in Eq. (10), which thereby yields the transition boundary

$$\lambda = \frac{3 - 4\eta^2}{\eta^4}. \tag{11}$$

The $\lambda = 0$ intercept of this transition occurs at $\eta = \sqrt{3}/2$, and $\eta \sim (3/\lambda)^{1/4} \to 0$ as $\lambda \to \infty$.

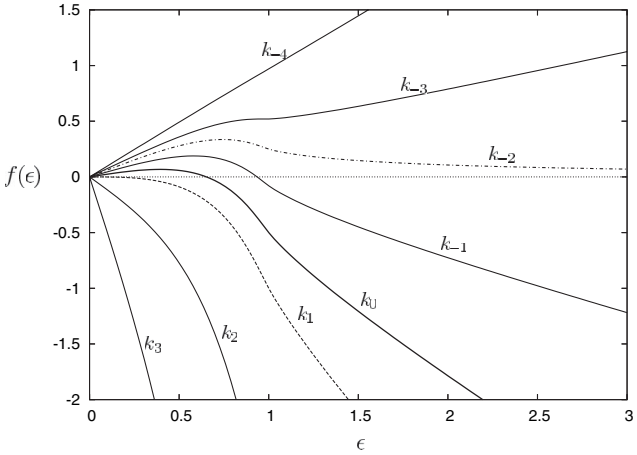

FIG. 1. Curves $f(\epsilon)$ for the composite disk at selected values of k. The curves shown are for $k_3 = 2.0$, $k_2 = 1.2$, $k_1 = \sqrt{2/3}$, $k_0 = 1/\sqrt{2}$, $k_{-1} = 0.60$, $k_{-2} = 1/2$, $k_{-3} = 0.40$, and $k_{-4} = 0.10$. The dashed curve for k_1 has zero slope at the origin; the dash-dot-dash curve for k_{-2} has zero slope at infinity; and the solid curve for $k_0 = 0.653$ corresponds to a pure disk.

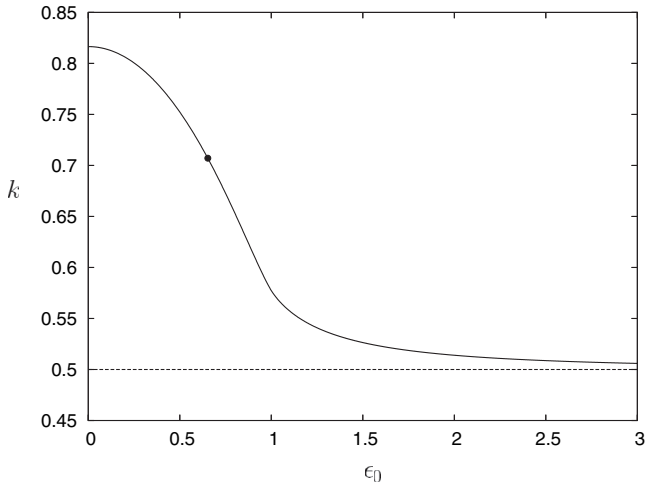

FIG. 2. The variation of k with terminal motion velocity ratio ϵ_0. The solid dot represents a pure disk.

The transition to terminal motion regime $\epsilon_0 = \infty$, obtained by setting $k = 1/2$ in Eq. (10), gives the transition boundary

$$\lambda = \frac{\eta^2 - 2}{\eta^4}. \tag{12}$$

The $\lambda = 0$ intercept of this transition occurs at $\eta = \sqrt{2}$ and there exists a turning point at $\lambda = 1/8$ where $\eta = 2$. Above the turning point $\lambda \sim 1/\eta^2 \to 0$ as $\eta \to \infty$. These transition boundaries are displayed in Fig. 3.

Scrutiny of the solutions shows that, mathematically, all three regimes exhibit the feature that rotation and translation stop simultaneously. This can be understood by examining the governing dynamical equations as $\epsilon \to 0$ and $\epsilon \to \infty$. For example, the series expansions for $K(\epsilon)$ and $E(\epsilon)$ in [6] give the leading developments $\mathcal{F}(\epsilon) \sim \epsilon$ and $\mathcal{T}(\epsilon) \sim 2/3$ as $\epsilon \to 0$. Inserting these results into (8a)

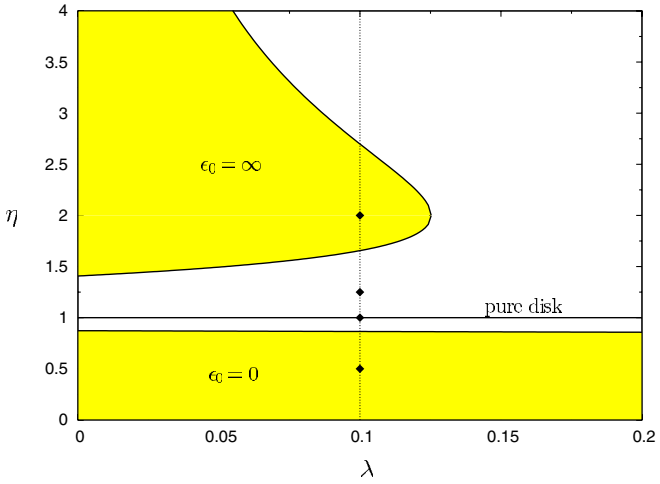

FIG. 3 (color online). Contours of ϵ_0 in λ-η space for the two-tier disk where solid diamonds show values of disks constructed.

and (8b) and solving the coupled equations gives the terminal translational and rotational velocity behaviors in the $\epsilon_0 = 0$ regime

$$v^* = C_1(t_f^* - t^*)^{3k^2/2}, \tag{13a}$$

$$\omega^* = \frac{2}{3k^2}(t_f^* - t^*), \tag{13b}$$

where C_1 is a constant and t_f^* is the common terminal time. Similarly, determination of the asymptotic behaviors of $\mathcal{F}(\epsilon)$ and $\mathcal{T}(\epsilon)$ as $\epsilon \to \infty$ may be used to find the terminal behaviors in the $\epsilon_0 = \infty$ regime

$$v^* = (t_f^* - t^*), \tag{14a}$$

$$\omega^* = C_2(t_f^* - t^*)^{1/4k^2}, \tag{14b}$$

where C_2 is a constant. From Eqs. (13) and (14), it can be seen that both v^* and ω^* are zero only at $t^* = t_f^*$. However, ω^* in (13) and v^* in (14) approach the zero point linearly with time, while their counterpart motions assume very small values before $t^* = t_f^*$.

To explore the terminal motion in the three regimes, we developed an experiment on a flat aluminum optical table 4 feet wide and 10 feet long. A Plexiglas sheet of uniform thickness 0.25 in. with planform dimensions 2×10 feet was fixed to the central section of the optical table using strips of double-sided adhesive tape less than 0.001 in. in thickness. Untreated nylon fabric was stretched tightly across the Plexiglas sheet and taped around its perimeter to the optical table. Motion was captured with an Olympus *i*-Speed camera at 100 frames/sec using an overhead mounting and a 45° mirror system. The camera imaged a foot-wide strip of the final four feet of the sliding surface illuminated by high intensity lamps.

Since the simple theory is predicated on disks having nearly uniform stress over the surface of contact, we need a criterion for its applicability. Effectively, the line of action of the normal force radially shifts a distance $\bar{R}$ from the center of mass toward the front of the disk due to the deceleration caused by sliding friction. Application of Newtonian dynamics gives this shift as

$$\bar{R} = \frac{\mu H_2}{2}\left(\frac{\eta^2\lambda^2 + 2\lambda + 1}{\eta^2\lambda + 1}\right) \tag{15}$$

and the stress over the contact surface will be nearly uniform when $\bar{R}/R_1$ is a small quantity.

TABLE I. Geometric characteristics of the two-tier disks used in the experiments.

	R_1 (in)	H_1 (in)	λ	η	k	$\bar{R}/R_1$	ϵ_0
disk 1	1.15	0.040	0.10	0.50	1.401	0.082	0
disk 2	2.00	0.875	0.10	1.00	0.707	0.171	0.653
disk 3	2.00	0.075	0.10	1.25	0.587	0.079	0.970
disk 4	2.20	0.100	0.10	2.00	0.482	0.081	∞

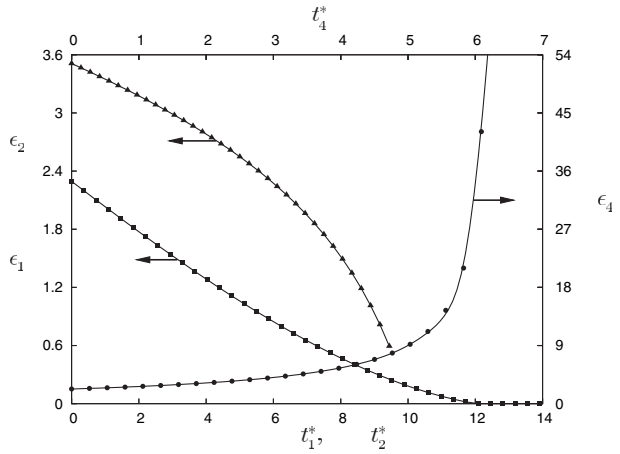

FIG. 4. Experimental data on the terminal behaviors of ϵ for disk 1 (squares), disk 2 (triangles), and disk 4 (circles). The solid lines are faired curves through the trajectory data.

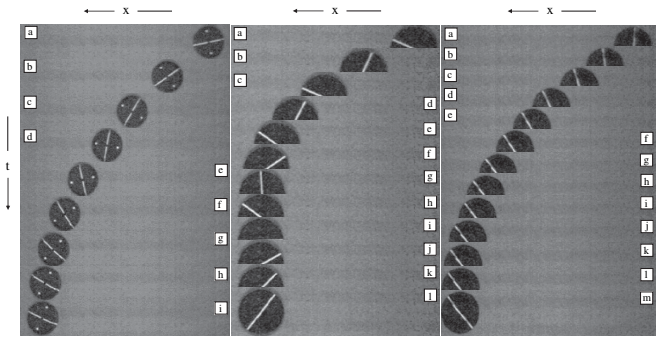

(a) disk 3 (b) disk 1 (c) disk 4

FIG. 5. Collages of the terminal motion of three disks. The horizontal expanse and time intervals between frames are: 29 in. and 0.67 sec for disk 3; 21 in. and 1.00 sec for disk 1; 27 in. and 0.43 sec for disk 4.

The solid diamonds in Fig. 3 and the tabulated values in Table I show the radius ratios η chosen to sample regions of terminal motion along the line $\lambda = 0.1$.

The composite disks were designed to have the same nominal value of $\bar{R}/R_1 \simeq 0.1$. The disks were fabricated from polyvinyl chloride (PVC) and their contact surfaces were sanded flat on a machinist's stone using successively finer grades of emery cloth. The actual dynamic friction coefficient, determined as the average of measurements made using all four disks, was $\mu = 0.39 \pm 0.05$. In addition to the geometrical disk properties listed in Table I, we have included the values of $\bar{R}/R_1$ (determined using $\mu = 0.39$) and the theoretical values of ϵ_0. We observed two forces acting on the sliding disks in addition to Coloumb friction. Static electricity built up after a PVC disk slid across the nylon surface. This effect was minimized by grounding the disk to the aluminum table before each run. A more serious concern was the stiction force that develops between closely mating surfaces. To minimize stiction effects, we selected a nylon fabric with a coarse weave and thus the value $\mu = 0.39$ quoted above. Although the stiction force must modify the motions of the disks, particularly in the terminal phase where the stiction has maximum effect due to the decreasing inertia of the disk, the disks seldom failed to stop in the terminal motion regime for which they were designed. Figure 4 gives experimental data for disks 1, 2, and 4, showing the evolution of ϵ with t^* near their terminal stopping points. The data in Fig. 4 offer only qualitative corroboration of the theory since the unknown contributions of stiction force and nonzero values of $\bar{R}$ are active.

Snapshots of the terminal motion for disks 1, 3, and 4 are shown in Fig. 5. Each collage contains identical sections of the table viewed from above as a disk travels right to left. Figure 5(a) shows composite disk 3 which simultaneously stopped sliding and spinning 0.23 sec after frame (h). Figure 5(b) shows composite disk 1 which stopped sliding 0.70 sec after frame (f) and ceased spinning 0.77 sec after frame (k). Figure 5(c) shows disk 4 which stopped spinning 0.23 sec after frame (g) and ceased sliding 0.13 sec after frame (l).

In conclusion, we note that multitiered disks also have terminal regime motions governed by k. In the limit as the tier heights become infinitesimally small, one approaches axisymmetric disk shapes with continuous section profiles which again have terminal motions governed by the normalized radius of gyration. Hence the present analysis is applicable to any axisymmetric geometry, devoid of holes, sliding and spinning with a flat area of contact. Results for disks with holes will be reported in a forthcoming publication.

P. D. W. extends his gratitude to Professor Bruno Keller for hospitality and support while at ETH Zürich. Thanks are extended to Eugen Magyari, Harry Thomas, Jim Meiss and Andrzej Herczynski for stimulating discussions on this problem.

[1] Z. Farkas, G. Bartels, T. Unger, and D. E. Wolf, Phys. Rev. Lett. **90**, 248302 (2003).
[2] D. Kadau, G. Gartels, L. Brendel, and D. D. Wolf, Phase Transit. **76**, 355 (2003).
[3] J. B. Knight, C. G. Fandrich, C. N. Lau, H. M. Jaeger, and S. R. Nagel, Phys. Rev. E **51**, 3957 (1995).
[4] M. Nicodemi, A. Coniglio, and H. J. Herrmann, Phys. Rev. E **55**, 3962 (1997).
[5] T. C. Halsey, Nature (London) **424**, 1005 (2003).
[6] M. Abramowitz and I. Stegun *Handbook of Mathematical Functions* (U. S. GPO, Washington, DC, 1972).
[7] S. Wolfram *Mathematica: A System for Doing Mathematics by Computer* (Addison-Wesley, Redwood City, CA, 1991).